MITSUBISHI ELECTRIC RESEARCH LABORATORIES
https://www.merl.com

A Unified Observer for Smooth Speed-Sensorless Drive Control of Induction Machines at Full Speed Range

Wu, Jingjie; Goldsmith, Abraham; Liu, Dehong; Wang, Bingnan; Zhou, Lei; Wang, Yebin

TR2025-060 May 20, 2025

Abstract

This paper proposes a novel unified observer that combines a modified low-frequency signal injection (LFSI) estimator and an adaptive full-order (AFO) flux observer for smooth sensorless control of nonsalient induction machines at full speed range. The unified observer adopts the same architecture as the AFO, i.e., comprising a rotor speed estimator and a flux observer. The speed estimator dynamics are enforced by an error signal from either the modified LFSI or the AFO, based on a switching signal indicating the system's observability at an operation point. In order to achieve a smooth transition during the switch, the LFSI channel is modified to enable the switching on the speed estimate derivative rather than the conventional approach of switching on the speed signal. A thorough theoretical analysis is provided. Simulations and experiments validate that the proposed unified observer results in smooth operation over the full speed range.

IEEE International Electric Machines and Drives Conference (IEMDC) 2025

Mitsubishi Electric Research Laboratories, Inc.
201 Broadway, Cambridge, Massachusetts 02139

A Unified Observer for Smooth Speed-Sensorless Drive Control of Induction Machines at Full Speed Range

Jingjie Wu
Wisconsin Electric Machines and Power Electronics Consortium
University of Wisconsin-Madison
Madison, USA
jingjie.wu@wisc.edu

Abraham Goldsmith
Mitsubishi Electric Research Laboratories (MERL)
Cambridge, MA 02139 USA
goldsmith@merl.com

Lei Zhou
Wisconsin Electric Machines and Power Electronics Consortium
University of Wisconsin-Madison
Madison, USA
lei.zhou@wisc.edu

Dehong Liu
Mitsubishi Electric Research Laboratories (MERL)
Cambridge, MA 02139 USA
liudh@merl.com

Bingnan Wang
Mitsubishi Electric Research Laboratories (MERL)
Cambridge, MA 02139 USA
bwang@merl.com

Yebin Wang
Mitsubishi Electric Research Laboratories (MERL)
Cambridge, MA 02139 USA
yebinwang@merl.com

***Abstract*—This paper proposes a novel unified observer that combines a modified low-frequency signal injection (LFSI) estimator and an adaptive full-order (AFO) flux observer for smooth sensorless control of nonsalient induction machines at full speed range. The unified observer adopts the same architecture as the AFO, i.e., comprising a rotor speed estimator and a flux observer. The speed estimator dynamics are enforced by an error signal from either the modified LFSI or the AFO, based on a switching signal indicating the system's observability at an operation point. In order to achieve a smooth transition during the switch, the LFSI channel is modified to enable the switching on the speed estimate derivative rather than the conventional approach of switching on the speed signal. A thorough theoretical analysis is provided. Simulations and experiments validate that the proposed unified observer results in smooth operation over the full speed range.**

***Index Terms*—Induction machine sensorless control, unified observer, low-frequency signal injection.**

I. Introduction

Induction machines (IMs) are widely used in industrial applications due to their simple construction, low cost, and low maintenance required. Indirect field-oriented control (IFOC) has enabled their excellent dynamic performance over a wide speed operation range [1], where a sensor such as an encoder is typically required to measure the rotor speed and thus estimate the rotor flux angle. However, the need for sensors can increase the system's cost and complexity, degrade overall reliability, and limit the applicability in harsh operating environments.

To overcome these challenges, speed sensorless control methods for IMs have gained considerable research attention in recent years. Prior sensorless control techniques can roughly be categorized into two main groups: the model-based approach and the signal-injection-based approach. The model-based method estimates the rotor flux angle and rotor speed according to the standard voltage model or full-order flux observer [2]. This approach can achieve satisfactory performance in medium-to-high speed operations but cannot maintain stability in zero or low-speed range, where speed observability becomes weak or even completely lost [3]. The signal-injection-based method typically injects a high-frequency voltage signal and analyzes the current response modulated by machine's saliency, such as inductance saturation, to estimate the rotor speed and field angle [4].

Although both sensorless techniques perform well within their respective operating conditions, neither is capable of achieving the full speed range sensorless control required in many applications. To overcome this limit, many studies try to enhance the robustness of the model-based approach at zero or low frequency. In [5], a new adaptive SMO full-order observer is proposed that uses independent gains for correction terms to improve the robustness and estimation accuracy at zero and very low frequencies. In [6], an enhanced magnetizing current-oriented low-frequency ride-through method is utilized to enable stable steady-state operation around zero synchronous speed. Despite the effectiveness, the fundamental limitations in strong sensitivity to model discrepancy and failure of continuous operations at low speeds remain unsolved. Another branch of research effort is avoiding zero-frequency (AZF) [7], [8], where the operating points are adjusted to avoid the unobservable operating regions. Nevertheless, there are operating conditions that cannot be modified by AZF in practice. Beyond these approaches, an intuitive idea is to combine model-based and signal-injection-based methods to achieve stable sensorless control over the full speed range. However, there is only limited work on this aspect for IM.

In [9], LFSI is used to enhance the flux observer at low speeds by combining the error signals with a weighted sum. In [10], a hybrid speed estimator that combines the model-based and injection-based speed estimation is utilized to enable sensorless operation at full speed range. Although effective, these combination approaches lack stability guarantee, can lead to nonsmooth transitions, and need significant tuning efforts.

In order to overcome the aforementioned challenges, this paper proposes a novel unified observer that consists of a modified LFSI observer and an adaptive full-order flux observer for non-salient induction machines. The error signals obtained from the modified LFSI and AFO are switched based on a switching signal indicating the observability of the system, which guarantees the stability over all operating conditions. The switched error signal is then used to compute the derivative of estimated rotor speed through a PI controller, making the speed estimation after an additional integration always smooth. The LFSI observer part is modified to enable the switching on the speed derivative rather than the speed itself in the conventional way. The parameters for switching can be readily selected by baseline AFO evaluations. Both simulation and experimental evaluations validate the LFSI controller design and demonstrate a smooth dynamic performance and the system's stability of the proposed unified observer over full speed range.

II. Preliminaries

A. Problem Statement

In the rotor flux-oriented dq reference frame where the d-axis is aligned with the rotor flux and the rotating synchronous speed is ω_s, the state-space model of an IM is given by

$$\begin{aligned} \dot{\boldsymbol{x}} &= \mathbf{A}(\omega_s)\boldsymbol{x} + \mathbf{B}\boldsymbol{v}_{dqs}, \\ \boldsymbol{y} &= \mathbf{C}\boldsymbol{x}, \end{aligned} \tag{1}$$

where

$$\boldsymbol{x} = \begin{bmatrix} \lambda_{ds} \\ \lambda_{qs} \\ \lambda_{dr} \end{bmatrix}, \quad \mathbf{A}(\omega_s) = \begin{bmatrix} \frac{-R_s}{L_s\sigma} & \omega_s & \frac{L_m R_s}{L_r L_s \sigma} \\ -\omega_s & \frac{-R_s}{L_s\sigma} & 0 \\ \frac{L_m R_r}{L_r L_s \sigma} & 0 & -\frac{R_r}{L_r\sigma} \end{bmatrix},$$
$$\mathbf{B} = \begin{bmatrix} 1 & 0 \\ 0 & 1 \\ 0 & 0 \end{bmatrix}, \quad \boldsymbol{v}_{dqs} = \begin{bmatrix} v_{ds} \\ v_{qs} \end{bmatrix}, \quad \boldsymbol{y} = \begin{bmatrix} i_{ds} \\ i_{qs} \end{bmatrix},$$
$$\mathbf{C} = \begin{bmatrix} \frac{1}{L_s\sigma} & 0 & -\frac{L_m}{L_r L_s \sigma} \\ 0 & \frac{1}{L_s\sigma} & 0 \end{bmatrix}.$$

Here $\lambda_{ds}, \lambda_{qs}$ are the stator fluxes in d- and q-axes; λ_{dr} is the rotor flux; R_s, R_r are the stator and rotor resistances; L_s, L_m, L_r are the stator, magnitizing and rotor inductances, respectively; $\sigma = \frac{L_s L_r - L_m^2}{L_s L_r}$ is the leakage factor; v_{ds}, v_{qs} are the input voltage in d- and q-axis; i_{ds}, i_{qs} are the stator current in d- and q-axes. Note that the q-axis rotor flux is always zero in this reference frame, i.e., $\dot{\lambda}_{qr} = \lambda_{qr} = 0$, which leads to the slip frequency and synchronous speed computations as

$$\omega_{\text{slip}} = \frac{L_m R_r}{L_r L_s \sigma} \frac{\lambda_{qs}}{\lambda_{dr}}, \tag{2}$$
$$\omega_s = \omega_r + \omega_{\text{slip}}, \tag{3}$$

where ω_r is the rotor electrical speed. The electromechanical equation of the IM is

$$\dot{\omega}_r = \frac{p}{J}(T_e - T_l), \tag{4}$$

where p is the number of pole-pairs, J is the rotor inertia, the friction is ignored, and the electromagnetic torque can be computed as

$$T_e = \frac{3p}{2}\frac{L_m}{L_r}\lambda_{dr} i_{qs}. \tag{5}$$

In conventional IFOC, we first compute the slip frequency using (2) and then derive the synchronous speed using (3) with ω_r measured by the speed sensor. Afterwards, the rotor flux angle can be readily obtained by integrating ω_s and used for Park transform to align with d-axis. Obviously, this approach fails in the sensorless case.

Therefore, the main objective of this paper is to estimate the rotor speed ω_r, reconstruct the state $\boldsymbol{x}$ in (1) and keep aligning $d-$axis with rotor flux correctly to generate the required torque (5) using only three-phase current measurements and commanded voltage.

Denote the estimated dq reference frame where actual dq current measurement and regulation take place by the subscript $\widehat{dq}$. Denote the position error between actual rotor flux frame and estimated $\widehat{dq}$ frame as $\tilde{\theta} = \theta - \hat{\theta}$.

B. Baseline Adaptive Flux Observer

As a baseline approach, the adaptive full-order flux observer in estimated $\widehat{dq}$ frame based on (1) can be constructed as follows

$$\begin{aligned} \dot{\hat{\boldsymbol{x}}} &= \mathbf{A}(\hat{\omega}_s)\hat{\boldsymbol{x}} + \mathbf{B}\boldsymbol{v}_{dqs} + \mathbf{L}(\boldsymbol{y}' - \hat{\boldsymbol{y}}), \\ \hat{\boldsymbol{y}} &= \mathbf{C}\hat{\boldsymbol{x}}, \end{aligned} \tag{6}$$

where $\hat{\boldsymbol{x}} = \begin{bmatrix} \hat{\lambda}_{ds} & \hat{\lambda}_{qs} & \hat{\lambda}_{dr} \end{bmatrix}^\top$ is the estimated stator and rotor fluxes; $\hat{\boldsymbol{y}} = \begin{bmatrix} \hat{i}_{ds} & \hat{i}_{qs} \end{bmatrix}^\top$ is the estimated $\widehat{dq}$-axis currents; $\boldsymbol{y}' = \begin{bmatrix} i_{\widehat{ds}} & i_{\widehat{qs}} \end{bmatrix}^\top$ is the current measurement in estimated $\widehat{dq}$-axis; $\mathbf{L} \in \mathbb{R}^{3\times 3}$ is the observer gain matrix. The error signal for estimating rotor speed is $e_{iqs} = i_{\widehat{qs}} - \hat{i}_{qs}$. Then, the estimated rotor speed, slip frequency, and synchronous speed can be estimated via a PI controller as follows

$$\dot{\hat{\omega}}_r = K_p(1 + \frac{K_i}{s})e_{iqs}, \tag{7}$$
$$\hat{\omega}_{sl} = \frac{L_m R_r}{L_r L_s \sigma}\frac{\hat{\lambda}_{\widehat{qs}}}{\hat{\lambda}_{\widehat{dr}}} + L_{42} e_{iqs}, \tag{8}$$
$$\hat{\omega}_s = \hat{\omega}_r + \hat{\omega}_{sl} \tag{9}$$

where L_{42} is an additional observer gain for slip frequency estimation. The rotor flux angle can be computed as

$$\hat{\theta} = \int \hat{\omega}_s \mathrm{d}t. \tag{10}$$

The flux and speed observer (6), (7) can achieve accurate speed estimation and stable sensorless operation at medium-to-high speed range. However, the speed estimation of this type of AFO typically becomes inaccurate or even diverges at low and zero frequencies, necessitating an alternative solution.

C. LFSI Observer

At zero-to-low frequency, the LFSI method is adopted to achieve sensorless operation. Rewrite the stator flux part of the model (1) in voltage and current form as:

$$\boldsymbol{v}_{dqs} = r_\sigma \boldsymbol{i}_{dqs} + \sigma L_s (s + \boldsymbol{J})\omega_s + E_{dqs}, \tag{11}$$

$$E_{dqs} = \frac{L_m}{L_r}\begin{bmatrix} -\frac{1}{\tau_r}\lambda_{dr} \\ \omega_r \lambda_{dr}, \end{bmatrix} \tag{12}$$

where $r_\sigma = R_s + \frac{L_m^2}{L_r \tau_r}$, $\tau_r = \frac{L_r}{R_r}$, $\mathbf{J} = \left[\begin{smallmatrix} 0 & -1 \\ 1 & 0 \end{smallmatrix}\right]$, s is the differential operator, E_{dqs} is the Back EMF in d- and $q-$axis.

When implementing LFSI, a low-frequency pulsating current $i^h_{\widehat{ds}} = i^h \cos(\omega^h t)$ is injected along the estimated $\hat{d}$-axis, which, in the true rotor flux reference frame, can be written as

$$\boldsymbol{i}^h_{dqs} = i^h \cos(\omega^h t)\begin{bmatrix} \cos(\tilde{\theta}) \\ -\sin(\tilde{\theta}) \end{bmatrix}. \tag{13}$$

Here, i^h is the injection magnitude and ω^h is the injection frequency. When a position estimation error $\tilde{\theta}$ exists, the q-axis component of i^h_{dqs} is nonzero, which generates a same-frequency torque ripple via (5) as

$$T^h = \frac{3p}{2}\frac{L_m}{L_r}\Big(\lambda_{dr} i^h_{qs} + \frac{L_m i^h_{ds}}{1 + s\tau_r} i_{qs}\Big). \tag{14}$$

From the dynamic model (4) neglecting friction and load, the speed perturbation induced by (14) can be computed as

$$\omega^h_r = \frac{3p^2}{2J}\frac{L_m}{L_r}\Big(\lambda_{dr}\frac{i^h_{qs}}{s} + \frac{L_m i^h_{ds}}{s(1 + s\tau_r)} i_{qs}\Big). \tag{15}$$

The speed perturbation further induces a back-EMF (BEMF) component with the same freuqency which can be used to estimate the rotor flux angle. Substitute (15) into (12) and transform from rotor-flux reference frame to the estimated $\widehat{dq}$ reference frame. The low-frequency BEMF in the estimated q-axis can be obtained as

$$v^h_{\mathrm{BEMF},\hat{\mathrm{q}}\mathrm{s}} = \frac{L_m^2}{L_r^2}\left(\omega_r R_r - k_\epsilon \tilde{\theta}\right)\frac{i_h \sin(\omega_h t)}{\omega_h} - O, \tag{16}$$

$$k_\epsilon = \left(\frac{3p^2\lambda_{dr}^2}{2J} + \frac{R_r}{\tau_r}\right), \tag{17}$$

$$O = \frac{3p^2 L_m^3 R_r i_{qs} \lambda_{dr}}{L_r^3 2J}\frac{i_h \cos(\omega_h t)}{\omega_h^2}, \tag{18}$$

where k_ϵ indicates the sensitivity from the position error to the BEMF of interest. The error signal to the phase-locked loop (PLL) is computed by demodulating the sinusoidal component as

$$\epsilon = \frac{1}{k_\epsilon}\left(\hat{\omega}_r R_r - \frac{L_r^2}{L_m^2}\mathrm{LPF}\Big[v^h_{\mathrm{BEMF},\hat{\mathrm{q}}\mathrm{s}}\frac{2\sin(\omega_h t)\omega_h}{i_h}\Big]\right), \tag{19}$$

where LPF denotes a low pass filter. Given accurate parameters, the equality $\epsilon = \tilde{\theta}$ holds, i.e., the error signal is equal to the position error. Then a PI controller within a PLL structure can be designed to ensure the alignment with rotor flux, i.e., $\tilde{\theta} \to 0$, and estimate rotor speed as follows

$$\begin{aligned} \hat{\omega}_s &= (K_p + \frac{K_i}{s})\epsilon, \\ \hat{\omega}_r &= \hat{\omega}_s - \frac{R_r L_m i_{\hat{q}s}}{L_r \hat{\lambda}_{dr}}. \end{aligned} \tag{20}$$

III. Unified Observer

In order to achieve speed-sensorless control over the full speed range, we propose the unified observer shown in Fig. 1, which combines the LFSI estimator operating at zero-to-low frequency range and the AFO operating at medium-to-high frequency range.

By comparing (20) and (7), we notice that the LFSI estimates the rotor flux speed while the AFO estimates the derivative of the rotor speed directly. Therefore, we propose various modifications to ensure a smooth transition between two observers during operations. First, the speed estimator of LFSI is modified as a regulator on the derivative of $\hat{\omega}_r$ to be consistent with (7) as

$$\begin{aligned} \dot{\hat{\omega}}_r &= (K_p + \frac{K_i}{s})\epsilon_{LFSI}, \\ \epsilon_{LFSI} &= C_{\mathrm{lead}}(s)\epsilon, \\ \hat{\omega}_s &= \hat{\omega}_r + \frac{R_r L_m i_{\hat{q}s}}{L_r \hat{\lambda}_{dr}}, \end{aligned} \tag{21}$$

where $C_{\mathrm{lead}}(s) = \frac{\alpha_c \tau s + 1}{\tau s + 1}$ is a lead compensator to make up for the extra $90°$ phase delay brought by integrating $\dot{\hat{\omega}}_r$ instead of directly obtaining $\hat{\omega}_r$. ϵ_{LFSI} is defined to be the new error signal. This is similar to controlling the position instead of speed for a motor. We further propose to replace the open-loop flux observer in LFSI method with the AFO so that the only difference lies in the way of generating the error signal in the speed estimator. Finally, the proposed unified observer can be represented as follows

$$\begin{aligned} &\dot{\hat{\boldsymbol{x}}} = \mathbf{A}(\hat{\omega}_s)\hat{\boldsymbol{x}} + \mathbf{B}\boldsymbol{v}_{dqs} + \mathbf{L}(\boldsymbol{y}' - \hat{\boldsymbol{y}}), \quad \hat{\boldsymbol{y}} = \mathbf{C}\hat{\boldsymbol{x}}, \\ &\dot{\hat{\omega}}_r = (K_p + \frac{K_i}{s})\epsilon^*, \quad \hat{\omega}_s = \hat{\omega}_r + \frac{L_m R_r}{L_r L_s \sigma}\frac{\hat{\lambda}_{\widehat{qs}}}{\hat{\lambda}_{\widehat{dr}}}, \\ &\epsilon^* = \begin{cases} e_{iqs}, & \text{if } |\hat{\omega}_s| \geq \delta \\ \epsilon_{\mathrm{LFSI}} \text{ from (21)}, & \text{otherwise} \end{cases} \end{aligned} \tag{22}$$

where δ is a user-defined switching threshold and the magnitude of $|\hat{\omega}_s|$ indicates the observability [3]. The combined error signal ϵ^* is switched between LFSI and AFO according to $|\hat{\omega}_s|$ and then goes through a PI regulator to output the derivative of estimated speed. Compared to switching on the speed estimate,

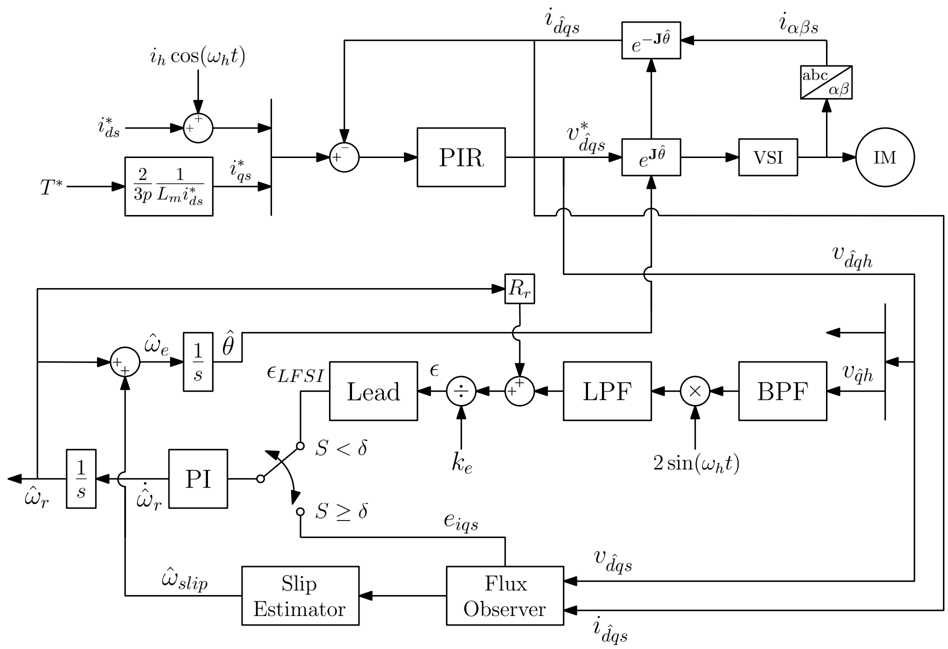

Fig. 1. Block diagram for unified observer in torque-controlled mode.

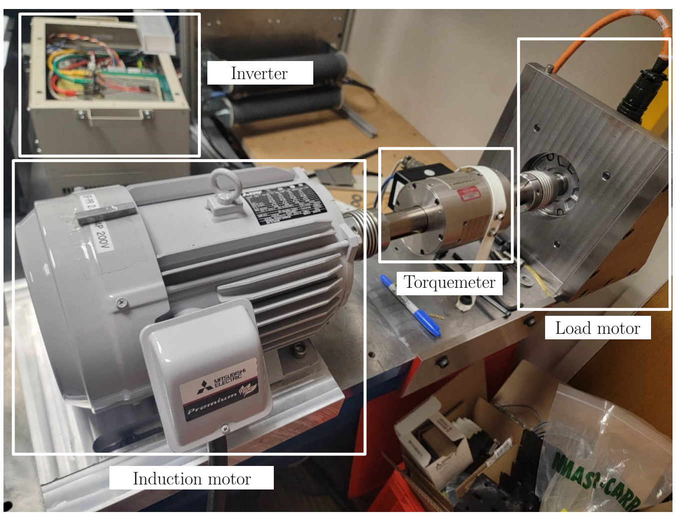

Fig. 2. Experimental testbed setup for IM.

switching on the estimated speed derivatives guarantees a smooth estimation during transition and the stability of the closed-loop system.

IV. Experiments

To fully demonstrate the performance of the proposed unified observer, this section presents the experimental results on an IM testbed as shown in Fig. 2. It consists of a MyWay AC-DC-AC three-phase inverter and a Mitsubishi Electric three-phase IM. The IM is coupled to an MR-J4 servomotor by a torque sensor. The IM is operating in torque-controlled mode while the servomotor is in speed-controlled mode. The nominal values of the IM's primary parameters

TABLE I
IM Parameters

Parameter	Nominal Value
Stator resistance R_s	0.428 Ω
Rotor resistance R_r	0.2839 Ω
Magnetizing inductance L_m	0.0601 H
Stator inductance L_s	0.0615 H
Rotor inductance L_r	0.0619 H
Moment of inertia J	0.015 kgm^2
Rated current I_b	6.5 A
Rated torque T_b	10 Nm
pole pairs p	2

are shown in the Table. I. During experiments, a dSPACE SCALEXIO LabBox executes the data acquisition, real-time estimation, controller implementation, and PWM generation. The sampling frequency and switching frequency are both 10 kHz.

The unified observer is implemented with switching threshold $\delta = 2$ Hz and benchmarked against the baseline AFO for comparison. Fig. 3 illustrates the results where the IM starts with 150 RPM and gradually decrease to 10 RPM with zero torque reference command. It can be observed from Fig. 3c and d that the baseline AFO cannot achieve a stable speed estimation and follow the torque command when approaching to low speed due to lack of observability. It can also be seen that the smaller the frequency, the larger oscillation the estimation has. This helps us determine the switching threshold as $\delta = 2$ Hz beyond which a decent performance is guaranteed with AFO part active. In Fig. 3a and b, the unified observer is able to obtain an accurate and smooth speed estimation over full-speed range and regulate the torque correctly around zero

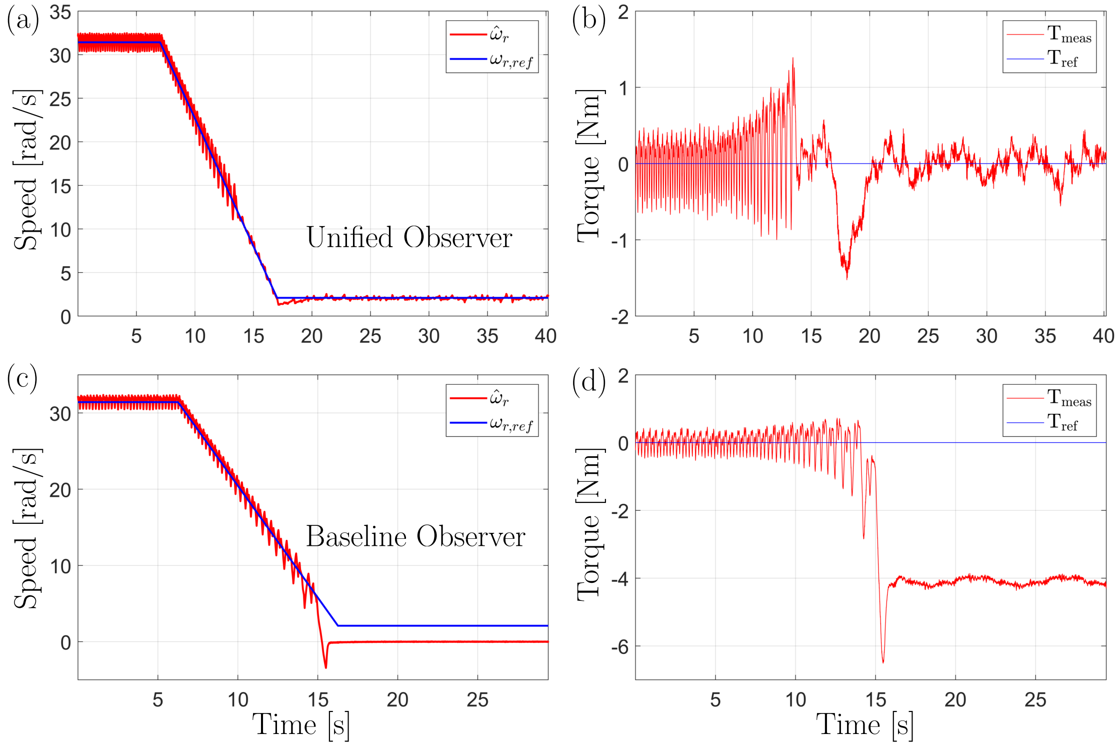

Fig. 3. Experimental results of test 1: from high speed to maintaining low frequency. (a) Speed response of unified observer. (b) Torque response of unified observer. (c) Speed response of baseline AFO. (d) Torque response of baseline AFO.

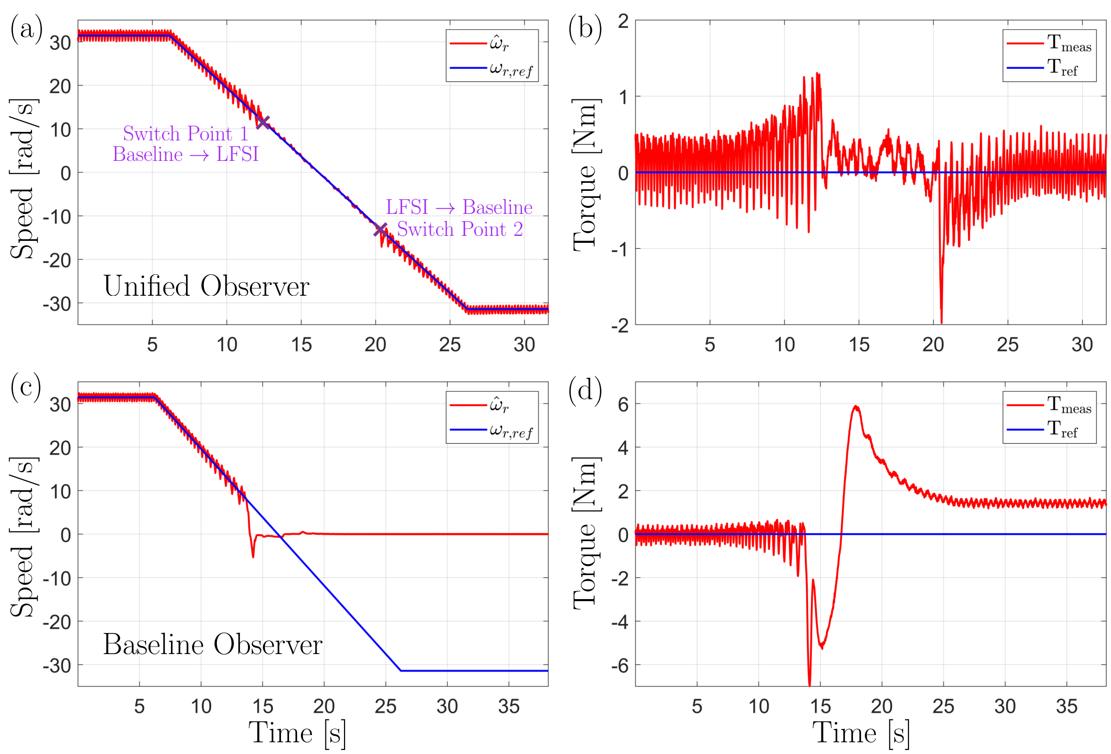

Fig. 4. Experimental results of test 2: from high speed to crossing zero frequency. (a) Speed response of unified observer. (b) Torque response of unified observer. (c) Speed response of baseline AFO. (d) Torque response of baseline AFO.

thanks to the proposed switching approach.

Fig. 4 shows another test where the IM starts with $150\ \mathrm{RPM}$ and is driven to $-150\ \mathrm{RPM}$ by load machine with zero torque reference command where two switch points are labeled. The AFO becomes unstable when the speed travels across zero and the torque significantly deviates from the reference command, which indicates a wrong alignment with rotor flux. On the other hand, the proposed unified observer is able to estimate the speed and regulate the torque through the two switches accurately and smoothly for the whole speed range, which demonstrates the effectiveness of our proposed algorithm.

V. Conclusion

This paper proposed a novel unified observer that combines a modified LFSI estimator and a baseline AFO for smooth sensorless control of IM at full speed range. The speed estimator dynamics of the unified observer are enforced by an error signal switched between LFSI and AFO, depending on a switching signal indicating the observability of the system at an operation point. Such a switching method guarantees the stability for all speeds and a smooth transition between the modified LFSI and AFO parts. Experimental evaluations show that the proposed unified observer can achieve accurate speed estimation over the full-speed range with a smooth and satisfactory dynamic performance, while the baseline AFO cannot provide stable control performances. Future works include applying the unified observer of a similar concept to salient IMs.

References

[1] D. W. Novotny and T. A. Lipo, *Vector control and dynamics of AC drives*. Oxford university press, 1996, vol. 41.

[2] S. Suwankawin and S. Sangwongwanich, "Design strategy of an adaptive full-order observer for speed-sensorless induction-motor drives-tracking performance and stabilization," *IEEE Transactions on Industrial Electronics*, vol. 53, no. 1, pp. 96–119, 2006.

[3] P. Vaclavek, P. Blaha, and I. Herman, "Ac drive observability analysis," *IEEE Transactions on Industrial Electronics*, vol. 60, no. 8, pp. 3047–3059, 2012.

[4] J. Holtz, "Sensorless control of induction machines—with or without signal injection?" *IEEE transactions on industrial electronics*, vol. 53, no. 1, pp. 7–30, 2006.

[5] M. S. Zaky, M. K. Metwaly, H. Z. Azazi, and S. A. Deraz, "A new adaptive smo for speed estimation of sensorless induction motor drives at zero and very low frequencies," *IEEE Transactions on Industrial Electronics*, vol. 65, no. 9, pp. 6901–6911, 2018.

[6] C. Luo, B. Wang, Y. Yu, Y. Zhu, and D. Xu, "Enhanced low-frequency ride-through for speed-sensorless induction motor drives with adaptive observable margin," *IEEE Transactions on Industrial Electronics*, vol. 68, no. 12, pp. 11 918–11 930, 2020.

[7] M. Depenbrock, C. Foerth, and S. Koch, "Speed sensorless control of induction motors at very low stator frequencies," in *8th European Power Electronic Conference (EPE)*, 1999, pp. 1131–1133.

[8] G. Lefebvre, J.-Y. Gauthier, A. Hijazi, X. Lin-Shi, and V. Le Digarcher, "Observability-index-based control strategy for induction machine sensorless drive at low speed," *IEEE Transactions on Industrial Electronics*, vol. 64, no. 3, pp. 1929–1938, 2016.

[9] M. Hinkkanen, V.-M. Leppanen, and J. Luomi, "Flux observer enhanced with low-frequency signal injection allowing sensorless zero-frequency operation of induction motors," *IEEE Transactions on Industry Applications*, vol. 41, no. 1, pp. 52–59, 2005.

[10] K. Ide, J.-I. H. J.-I. Ha, M. Sawamura, H. Iura, and Y. Yamamoto, "A novel hybrid speed estimator of flux observer for induction motor drives," in *Industrial Electronics, 2002. ISIE 2002. Proceedings of the 2002 IEEE International Symposium on*, vol. 3. IEEE, 2002, pp. 822–827.